Small Angle Neutron Scattering Studies on Miscible Blends of Poly(styrene-*ran*-vinyl phenol) with Liquid Crystalline Polyurethane

Rujul Mehta[†] and M. D. Dadmun*[,†,‡]

Department of Chemistry, University of Tennessee, Knoxville, Tennessee 37996, and Chemical Sciences Division, Oak Ridge National Laboratory, Oak Ridge, Tennessee 37831

Received May 9, 2006; Revised Manuscript Received August 19, 2006

ABSTRACT: The production of uniformly dispersed rigid-rod liquid crystalline polymer (LCP) molecules in a flexible amorphous polymer, with an experimentally accessible miscibility window, has become possible by modifying the architecture of the flexible polymer, so as to induce favorable inter-species hydrogen bonding. The conformation of LCP chains that are uniformly dispersed in a flexible coil matrix are examined by studying a system consisting of a liquid crystalline polyurethane (LCPU) and a copolymer containing 12% vinylphenol and deuterated styrene, utilizing small-angle neutron scattering. Intramolecular hydrogen bond interaction within the vinylphenol segments of the copolymer leads to the formation of a dynamically cross-linked structure, characterized by the large amount of scattering seen at low angle. Addition of the LCPU in the blend results in formation of hydrogen bonding interactions between the LCP and the copolymer; demonstrated by an initial reduction in the correlated size of the dynamic network at the lowest LCP dosage, whereas the network size is recovered in blends containing higher amounts of the LCPU. Using FTIR to quantify the amount of intramolecular hydrogen bonding between the polymers, the results demonstrate the conversion from intra-species to inter-species hydrogen bonding; further corroborating the observation that the LCPU molecules integrate themselves into the hydrogen bonded physical network. Investigation of the high-angle portion of the scattering curves reveals that the LCPU molecules exhibit presence of anisotropic structures staggered along its length, resulting in rods that are shorter and thicker than a fully extended LCPU chain. With increasing concentration of the LCPU, interference between individual LCP molecules leads to orientation and structures with greater lengths of the anisotropic portions, leading up to formation of anisotropic aggregates that contain multiple LCPU molecules.

Introduction

Liquid crystals[1] and liquid crystalline polymers[2] (LCP) form an important class of high performance materials, with applications that utilize their unique anisotropic optical, electrical, and, especially in the case of the latter, mechanical properties.[3−5] Broad commercial utilization of these materials has been limited by their high costs.[6] Consequently, blends of rigid liquid crystals with random coil amorphous polymers have been prepared. Generally, this gives rise to inhomogeneous mixtures of liquid crystals and flexible coil polymers (polymer dispersed liquid crystals), which are of interest due their applications in electrooptical devices.[7−10] On the other hand uniformly dispersed rigid-rod LCP molecules in a flexible amorphous polymer matrix, known as molecular composites,[11−13] can synergistically combine desirable properties of the flexible coil matrix and rigid rod segments of the LCP, to produce superior materials with extraordinary structural properties, thermal stability, processability, and toughness.[14−16]

Unfortunately, molecular composites have remained hitherto elusive, due to a scarcity of miscible systems containing a LCP and an amorphous polymer. A successful route toward preparation of a molecularly dispersed LCP-flexible polymer blend involves introduction of strong specific interactions between the two species, including hydrogen bonding or strong dipole−dipole interactions[17−24] and ionic interactions.[25−29] As the result of recent work by Vishwanathan and Dadmun,[17] the production of such a blend, with an experimentally accessible miscibility window, has become possible by modifying the architecture of the flexible polymer, so as to induce optimal favorable inter-species hydrogen bonding. Specifically, liquid crystalline polyurethanes (LCPU) are found to have a significant miscibility window with a copolymer of styrene and vinylphenol[13,18−20] (VPh) with optimum hydrogen bonding between the carbonyl groups of the urethane linkages and the hydroxyl groups present in the styrenic matrix. Moreover, this optimization occurs when the hydroxyl groups are separated along the copolymer chain, simply by varying the composition of the copolymer. Improvement of the rotational freedom of the functional groups participating in hydrogen bonding and reduction in the probability of intra-species hydrogen bonding with increased spacing between the hydroxyl groups impacts the extent of hydrogen bonding and correspondingly, the miscibility window.[18,20] It has been found that the broadest miscibility window can be realized for a system containing 10−20% VPh in the copolymer, which is also the system that shows optimum amount of inter-species hydrogen bonding as shown by Fourier transform infrared spectroscopy (FT-IR).

Availability of a truly miscible molecular composite presents a unique opportunity of studying the conformation of polymer chains containing rigid rods that are uniformly dispersed in a flexible coil matrix. This information is of great importance, as it will provide a direct correlation of the molecular structure of the LCP and the coillike polymer to the macroscopic properties of the blend. A unique feature of LCP materials is their readiness to form a spontaneously ordered phase via anisotropic interactions within its rigid rods.[30,31] This tendency governs the miscibility of such systems. Coleman and Painter[32] have theoretically estimated that single-phase rod/coil mixtures can be obtained if there exists strong specific interactions between the rods and the coil. They have also correlated the tendency of the two polymers to mix in the presence of specific interactions to the chemical similarity of the rods to the coil.

* Corresponding author.
[†] Department of Chemistry, University of Tennessee.
[‡] Chemical Sciences Division, Oak Ridge National Laboratory.

10.1021/ma0610360 CCC: $33.50
Published on Web 11/10/2006

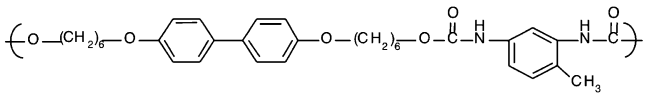

Figure 1. Molecular structure of liquid crystalline polyurethane (LCPU).

The determination of the state of conformation of molecularly dispersed LCP in a coiled polymer can provide crucial information that can be utilized to account for the range of anisotropy present of polymers in polymer blends beyond rigid rod polymers.

To gain fundamental insight into the configuration of the LCPU molecules in an amorphous matrix, we have utilized small-angle neutron scattering (SANS).[33−39] The advantage of SANS is that the conformation of polymer molecules can be determined at any concentration, as scattering contrast can be tuned by selective deuteration of one of the components.[33,38] A system consisting of the LCPU and a deuterated styrenic copolymer containing 12% VPh was examined by SANS. The structure of the LCPU is shown in Figure 1.

The low angle-portion of the curve indicates the presence of a hydrogen bonded dynamic network, whose dimensions are determined by a Debye−Bueche type analysis[40] as well as Kratky and Zimm models, modified to account for the presence of such a network.[41] The rigidity of the LCP chain in the amorphous matrix was determined by Kratky analysis with fitting of the high-angle portion of the curve to the Kratky−Porod wormlike chain model.[42]

Experimental Section

Materials. 4,4 Bisphenol and 2,4-toulene diisocyanate were obtained from TCI America Inc.; styrene-d_8 was obtained from Polymer Source Inc.; 4-acetoxystyrene, tetrahydrofuran, and hydrazine hydrate were purchased from Aldrich Chemical Co.; and methanol, dioxane, and *N*,*N*′-dimethylformamide (DMF) were purchased from Fisher-Acros.

Polymer Synthesis and Characterization. The liquid crystalline polyurethane (LCPU) was prepared by condensation of 4,4-biphenol and 2,4-toulene diisocyanate.[17,18,20,43] Poly(styrene-d_8-*co*-4-vinylphenol) (Pd_8S-*co*-VPh) random copolymers were synthesized in two batches, by atom transfer radical polymerization, using phenoxybenzene-4,4′-disulfonyl chloride as the initiator and a copper chloride/2,2′-bipyridine complex as the catalyst;[44,45] followed by hydrolysis of the acetoxy groups using hydrazine hydrate and dioxane according to the procedure of Green and Khatri.[23]

The molecular weights of the polymers were determined using a Polymer Laboratories PL-GPC 20 gel permeation chromatograph (GPC) equipped with two PLGel 5 μm Mixed C columns and a refractive index detector. DMF was used as elution solvent for the LCPU and tetrahydrofuran for Pd_8S-*co*-VPh copolymer. Polystyrene with a narrow molecular weight distribution was used as calibration standard for all polymers. Whereas the molecular weights of the two batches of Pd_8S-*co*-VPh copolymer were $M_w = 70200$, PDI = 1.65 and $M_w = 55700$, PDI = 1.42, the molecular weight of the LCPU was $M_w = 31700$, PDI = 1.64. The copolymer composition was determined by oxygen content in the copolymers. The elemental analysis was performed by Atlantic Microlab Inc. The Pd_8S-*co*-VPh copolymer contained 12% VPh segments.

Sample Preparation. Blends of LCPU and Pd_8S-*co*-VPh copolymer were prepared in solution of DMF and subsequently precipitated in excess of cold methanol. The precipitate was separated by centrifuge and dried in a vacuum oven at 150 °C in excess of 24 h. Dried polymer blends were compression molded at 150 °C, to form sample preforms in the shape of cylindrical disks. These disks were then pressed between two quartz disks separated by a spacer of 1 mm thickness, to ensure uniform path thickness of 1 mm. Blends were prepared having compositions, 0.5−5%, and 20% weight fraction of LCPU in the blend.

SANS Measurements. The small-angle neutron scattering (SANS) measurements were carried out in two series. The first measurements were performed on compositions of 5% and 20%, using the instrument NG3, at the National Center for Neutron Research of the National Institute of Standard and Technology (NIST), at Gaithersburg, MD. The fixed-wavelength 30 m long pinhole instrument was operated at a wavelength, $\lambda = 6$ Å, 180 °C over a scattering vector range of $0.0034 < Q < 0.11$ Å^{-1}.

A second set of the experiments were carried over the composition range of 0.5 to 3%, at the Institute of Solid State Research (IFF) of at the Forschungszentrum in Jülich, Germany, using the instrument KWS1. This instrument is a 40 m pinhole instrument operating on the wavelength of $\lambda = 7$ Å, and scattering data was obtained over the Q range 0.0023−0.16 Å^{-1} and at 170 °C.

The scattering data was corrected for empty cell scattering, detector sensitivity, and background scattering, and subsequently normalized to absolute scattering intensity using a poly(methyl methacrylate) standard. The scattering patterns were radially averaged to obtain the absolute scattered cross section $d\Sigma(Q)/d\Omega$ vs scattering vector Q, where $Q = (4\pi/\lambda)\sin(\theta/2)$. Contributions due to incoherent scattering and thermal fluctuations were determined by plotting[46] $[Q^4 d\Sigma(Q)/d\Omega]$ vs Q^4. At large scattering vector Q, this plot is linear and its slope gives the magnitude of the sum of incoherent and thermal scattering contributions. The magnitude of this slope was always less than 5 cm^{-1} and was subtracted from the data.

FT-IR Measurements. Infrared spectra were obtained on a Biorad FTS-60A Fourier transform infrared (FT-IR) spectrometer at 25 °C, purged with dried air using a minimum of 256 scans over a range of 4000−400 cm^{-1} wavenumber, at a resolution of 2 cm^{-1}. The frequency scale was internally calibrated with a He−Ne reference to an accuracy of 0.2 cm^{-1} and externally with polystyrene. Samples for the FT-IR study were prepared by solvent casting of Pd_8S-*co*-VPh/ LCPU blends from 2% (w/v) DMF solutions on polyethylene IR cards (purchased from International Crystal Laboratories). After most of the solvent was evaporated off at room temperature, the IR cards were subsequently dried in a vacuum oven at 70 °C for over 1 day to remove residual solvent and moisture.

Results and Discussion

Copolymer. Figure 2 shows the absolute scattering intensities obtained from the pure Pd_8S-*co*-VPh random copolymer and its blends containing 5% and 20% LCPU at 180 °C. Scattering curves of neat copolymer shows a remarkable upturn in scattering at low Q. The slope of the scattering curve in log−log representation, in the low Q limit (<0.026 Å^{-1}), is approximately −3.6. It is evident that the vinylphenol (VPh) monomer segments, (which were not deuterated), in the random copolymer form a large-scale structure, facilitated by the presence of hydrogen bonding among them. This interaction in the VPh segments leads to formation of a dynamically cross-linked structure, characterized by the large amount of scattering seen at low Q. The Debye−Bueche model is normally used to describe scattering from a random two-phase system but it can also be applied to random copolymers where one comonomer is segregated from the other.[47]

The Debye−Bueche model is based on the correlation function γ[40]

$$\gamma(r) = \exp\left(-\frac{r}{\xi}\right) \tag{1}$$

where ξ is the correlation length. The Fourier transform of the Debye−Bueche model appears as

$$\frac{d\Sigma}{d\Omega}(Q) = \frac{d\Sigma}{d\Omega}(0)\frac{1}{(1 + Q^2\xi^2)^2} \tag{2}$$

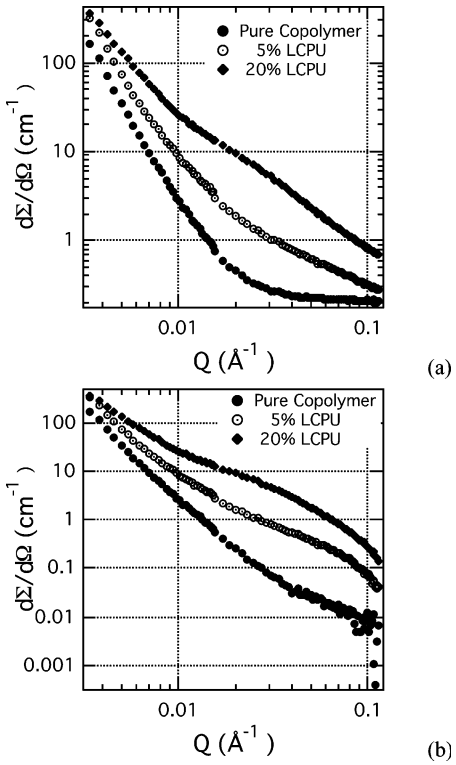

Figure 2. Small-angle neutron scattering (SANS) intensity for Pd_8S-*co*-VPh copolymer and its blends containing 5% and 20% LCPU at 180 °C, in double logarithmic scale and absolute units: (a) before and (b) after subtracting the incoherent portion of the scattering.

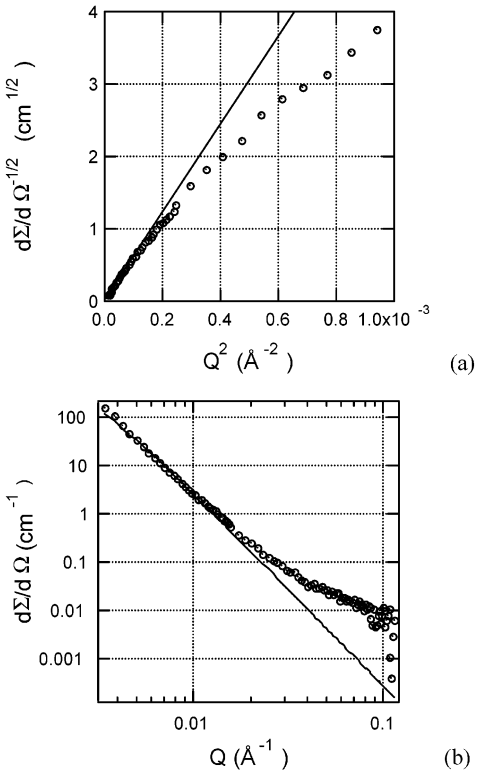

Figure 3. (a) Inverse root of SANS intensity for the neat Pd_8S-*co*-VPh copolymer as a function of Q^2, to obtain the linear fit (—) to the Debye−Bueche model, and (b) comparison of the scattering intensity to the intensity predicted by the Debye−Bueche model (—) in double logarithmic scale.

for which it is customary to plot $[d\Sigma(Q)/d\Omega]^{-1/2}$ vs Q^2 (Figure 3a). Figure 3b shows that the scattering curve for neat Pd_8S-*co*-VPh copolymer fits reasonably well to the Debye−Bueche model in the low Q range (<0.026 Å^{-1}). In the copolymer there is strong hydrogen bonding interaction between the VPh units leading to formation of a long-range dynamic network. This results in the presence of fluctuation in the local concentration of VPh at the hydrogen bonding sites. The correlation length ξ of 35.5 nm obtained from this fit, represents the length scale over which neighboring vinylphenol aggregates that form nodes of the network are correlated across the dynamic network.

At higher Q (>0.026 Å^{-1}), the slope of the scattering curve in log−log representation is approximately −2, indicating a Gaussian distribution of the VPh segments over smaller length scales. The Debye form factor describes the scattering of a Gaussian distribution of scattering centers, for which the scattering function is[48]

$$\frac{d\Sigma}{d\Omega}(Q) = \frac{\phi m}{N_A \delta}(\Delta\rho)^2 \left\{ \frac{2[\exp(-\omega N) + \omega N - 1]}{\omega^2 N} \right\} \quad (3)$$

where $\omega = Q^2b^2/6$, b is the mean square size of the scattering center, m is its molecular weight, ϕ is volume fraction, N is the number of scattering centers in a scattering structure, N_A is Avogadro's number, δ is the density, and $\Delta\rho$ is the scattering length density contrast. In the high Q limit eq 3 simplifies to

$$\frac{d\Sigma}{d\Omega}(Q) \approx \frac{\phi m}{N_A \delta}(\Delta\rho)^2 \frac{2}{\omega} = 12 \frac{\phi}{N_A \delta}(\Delta\rho)^2 \frac{m}{Q^2 b^2} \quad (4)$$

This relationship is visualized by plotting the second moment of the intensity, $[Q^2 d\Sigma(Q)/d\Omega]$ vs Q, also known as the Kratky plot. In Figure 4, the scattering data for the neat Pd_8S-*co*-VPh copolymer in the Kratky representation appears as a plateau in the high Q range (represented by the dotted line).

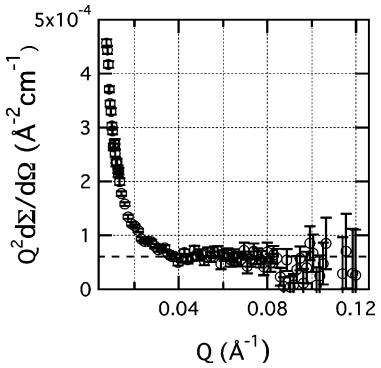

Figure 4. Kratky plot or the second moment of SANS intensity for neat Pd_8S-*co*-VPh copolymer as a function of Q, showing a linear plateau (- -) at high Q corresponding to the linear chain segments of the network.

The asymptote gives the value, $b = 8.98$ nm, which is the statistical segment length of the Gaussian distribution of vinylphenol units. It is clearly seen that the Kratky plot approaches its asymptote from above, which is a signature of network polymers. Benoit and co-workers[41] have modified eq 3 to account for branched or cross-linked polymers:

$$\frac{d\Sigma}{d\Omega}(Q) = \frac{\phi m}{N_A \delta}(\Delta\rho)^2 \left\{ \frac{2}{\omega} + \frac{1}{n\omega^2}\left[f - 2 - \frac{f}{s} \right] \right\} \quad (5)$$

where s is the number of branches or inter-node segments containing n repeat units ($N = ns$), and f is the functionality (f branches start from each cross-link).

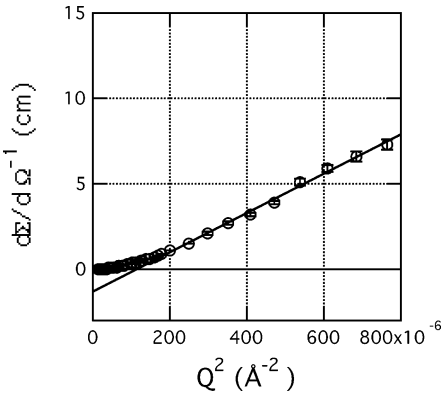

Figure 5. Inverse of SANS intensity for neat Pd_8S-*co*-VPh copolymer as a function of Q^2, showing a linear fit (—) at high Q to the modified Zimm plot according to eq 8. Note the negative intercept, which is an indicator of presence of networking in the copolymer.

The fraction of associated hydroxyl groups p in a hydrogen bonded network[49]

$$p = 1 - \frac{\phi_{VPh,f}}{\phi_{VPh}} = \phi_{VPh,f}\left[\left(1 - \frac{K_2}{K_B}\right) + \frac{K_2}{K_B}\left(\frac{1}{(1 - K_2\phi_{VPh,f})}\right)\right]^{-1} \tag{6}$$

where ϕ_{VPh} is the fraction of monomer units having hydroxyl groups (i.e., vinylphenol content, 0.12 in our case), $\phi_{VPh,f}$ is the fraction of monomer units that are not associated through any hydrogen bonding. K_2 and K_B are the self-association equilibrium constants for formation of the hydrogen bonds between phenol units, involving two or more VPh units, respectively. Using the equilibrium constants at 170 °C, this relationship yield value of $p = 0.18$, which means that at any given time 82% of vinylphenol units are free from hydrogen bonding. Further, the fraction of vinylphenol aggregates consisting of x vinylphenol units can be further obtained by the probability $p^{x-1}(1 - p)$, indicating that dimers containing a single hydrogen bond between two vinylphenol units is the most common type of cross-link present in the network. In other words almost all cross-links involve only two chain segments, leading to the functionality of $f = 4$. Hence the number s of branches becomes large, f/s can be neglected with respect to $f - 2$, and eq 5 simplifies to

$$\frac{d\Sigma}{d\Omega}(Q) = \frac{\phi m}{N_A\delta}(\Delta\rho)^2\left[\frac{2}{\omega} + \frac{2}{n\omega^2}\right] \tag{7}$$

or

$$\frac{d\Sigma}{d\Omega}^{-1}(Q) = \frac{N_A\delta}{\phi m}\frac{1}{(\Delta\rho)^2}\left[\frac{\omega}{2} - \frac{1}{2n}\right] = \frac{N_A\delta}{\phi m}\frac{1}{(\Delta\rho)^2}\left[\frac{Q^2b^2}{12} - \frac{1}{2n}\right] \tag{8}$$

prompting the plotting of the data in the Zimm representation $\{[d\Sigma(Q)/d\Omega]^{-1}$ vs $Q^2\}$. Figure 5 shows the Zimm plot of the scattering data has a linear fit with a negative intercept that gives

$$b^2 = 12\frac{\phi m}{N_A\delta}(\Delta\rho)^2 \times \text{gradient} \tag{9}$$

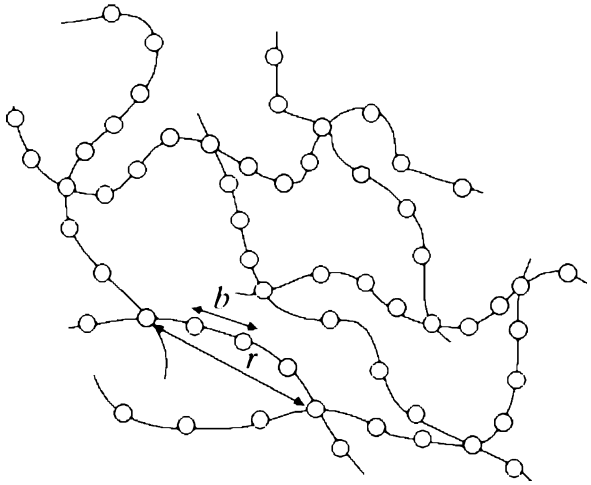

Figure 6. Schematic diagram showing a physically cross-linked copolymer. The circles in the diagram denote VPh monomer units.

and

$$n = \frac{N_A\delta}{\phi m}\frac{1}{(\Delta\rho)^2} \times \frac{-1}{2 \times \text{intercept}} \tag{10}$$

The Pd_8S-*co*-VPh copolymer is a statistical copolymer, where VPh monomer units are randomly interspersed in a chain composed of deuterated styrene monomer units. Through hydrogen bonding, the VPh units form physical "cross-links", thereby bringing together the copolymer chains to form a large network with each interlink composed of a random sequence of VPh and styrene-*d* monomer units. This simple model is shown in a schematic diagram in Figure 6. The scattering produced by the copolymer arises from sequences of protonated VPh monomer units, which are separated by runs of deuterated styrene monomer units. As a result, the scattering results from a random walk, where a statistical segment contains multiple VPh monomer units and the step length of the random walk is the statistical segment length of the vinylphenol units b.

The linear fit in Figure 5 yields the number of statistical segments per branch or interlink as $n = 9.19$ and the length of each statistical segment as $b = 8.04$ nm, which is comparable with $b = 8.98$ nm obtained from eq 4. In other words, on average one in nine VPh statistical segment is involved in a physical link. The end-to-end distance between two linkages can be obtained by multiplying eqs 9 and 10; $r = n^{1/2}b = 24.38$ nm and radius of gyration of an interlink is $r_g = n^{1/2}b/6^{1/2} = 9.96$ nm. Because of the presence of the network, it is not possible to deduce the molecular weight or radius of gyration of a single copolymer chain from the SANS data, but it is reasonable to assume that the dimensions of a single copolymer chain would be intermediate between the radius of gyration of one interlink $r_g = 9.96$ nm and correlation length ξ of 35.5 nm obtained from the Debye−Bueche model.

Blends. Figure 7 shows the scattering intensities obtained from pure Pd_8S-*co*-VPh copolymer and its blends plotted in the Kratky representation. What is interesting to observe in these curves is the additional scattering that occurs in the blends. The scattering data from the Pd_8S-*co*-VPh copolymer/ LCPU blends show a clear deviation from the plateau at high Q. This excess scattering that is not present in the data for the pure copolymer evidently contains the information regarding the conformation of the LCP molecules. The bell-shaped peak seen in Kratky plot is an indication of the presence of rodlike structures[50−52] in the polymer blends.

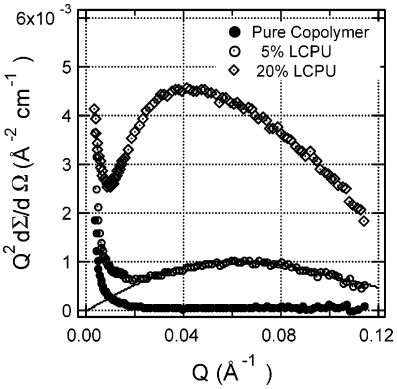

Figure 7. SANS intensity for blends of Pd_8S-*co*-VPh copolymer containing 5% and 20% LCPU showing excess scattering occurring at $Q > 0.016$ Å^{-1}, when compared with scattering from pure copolymer (also shown). The solid curve (—) corresponds to the fit of the scattering data for 5% blend to the Kratky−Porod wormlike chain (KPWC) model (eq 11) presented in Kratky representation.

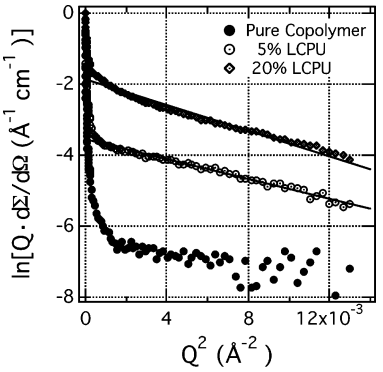

Figure 8. Logarithm of the first moment of SANS intensity for 5 and 20% LCPU−Pd_8S-*co*-VPh copolymer blends as a function of Q^2, to obtain linear fits (—) to the Kratky−Porod wormlike chain model. Data for the pure copolymer is also shown which does not exhibit a strong linear behavior.

The scattering arising from anisotropic structures is better represented by a model based on a form factor for a cylinder of cross-sectional radius of gyration $R_{g,x}$and length L, given as

$$\frac{d\Sigma}{d\Omega}(Q) = \frac{\pi\phi(\Delta\rho)^2}{N_A\delta}\frac{M}{L}\frac{1}{Q}\exp\left(\frac{-Q^2R_{g,x}{}^2}{2}\right) \qquad (11)$$

or

$$Q^2\frac{d\Sigma}{d\Omega}(Q) = \frac{\pi\phi(\Delta\rho)^2}{N_A\delta}\frac{M}{L}Q\exp\left(\frac{-Q^2R_{g,x}{}^2}{2}\right) \qquad (12)$$

where M is the molecular weight of the cylinder. This relation (eq 11) is known as the Kratky−Porod wormlike chain (KPWC) model. KPWC model describes scattering arising from a cylinder and is applied to systems containing anisotropic structures.[33,34,38,42] Figure 7 shows the fit obtained from eq 12 to the scattering data from the blend containing 5% LCPU. It is seen that eq 12 fits well to the scattering data in the high Q limit. As a result, this scattering data can be displayed in a linear form by plotting $\ln[Qd\Sigma(Q)/d\Omega]$ vs Q^2 (Figure 8). The cross-sectional radii of gyration $R_{g,x}$ obtained from this fit are 1.72 and 1.69 nm for 5% and 20% LCPU blends respectively, whereas $R_{g,x}$ obtained from fitting 5% LCPU blend data to eq 12 (Figure 7) is 1.60 nm. Assuming that the scattering observed from the blends in the high Q region (>0.026 Å^{-1}), over which eq 11 and (12) are fitted, arises from LCPU molecules dispersed in the copolymer matrix; $R_{g,x}$ serves as an indication of the cross-sectional size of the anisotropic structures. The intercept to the straight line fit in Figure 8 provides the ratio M/L, which is a measure of the molecular weight per unit length along the anisotropic structure, with values of 436 and 572 g mol^{-1} nm^{-1} for 5% and 20% LCPU blends, respectively.

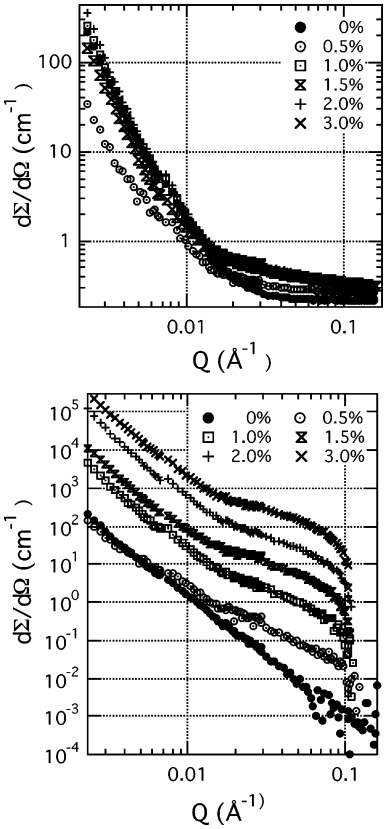

Figure 9. SANS intensity for Pd_8S-*co*-VPh copolymer and its blends containing 0.5−3% LCPU at 170 °C, in double logarithmic scale and absolute units: (a) before and (b) after subtracting the incoherent portion of the scattering. Data in part b are offset for clarity.

Blends Containing Low LCPU Content. Although the correlation of the scattering data to the KPWC model indicates that the excess high Q scattering occurring in the blends is from LCPU molecules, there remains the possibility that the LCPU molecules themselves enter the hydrogen-bonded dynamic network formed within the Pd_8S-*co*-VPh copolymer matrix. Therefore, a correlation between different LCPU molecules cannot be ruled out. In other words, the high concentration of the LCPU within the blend may result in interference between different LCPU molecules. With these considerations, a second series of SANS experiments were carried out exclusively on blend concentrations varying from 0.5 to 3 wt % fraction of LCPU as well as the neat copolymer. Figure 9 shows the absolute scattering intensities obtained from pure Pd_8S-*co*-VPh copolymer and its blends containing 0.5%, 1.0%, 1.5%, 2.0%, and 3.0% LCPU at 170 °C. Scattering curves of the neat copolymer and the blends show the same upturn in scattering at low Q observed in Figure 2.

As before, the scattering data in the low Q limit was fitted to the Debye−Bueche model, i.e., eq 2. The correlation length obtained from this fitting procedure is presented in Table 1. The addition of small amounts of LCPU in the scattering media results in a measurable change in the character of the scattering. At the lowest LCPU dosage, a substantial reduction in the scattering is observed within the low-Q range (curve due to 0.5%); indicating that the LCPU molecules act to disrupt the

Table 1. Debye−Bueche Model Fitting Parameters for a Low *Q* SANS

LCPU wt fraction (%)	ξ (nm)	$(d\Sigma/d\Omega)(0)$ (cm^{-1})
0	$27.3 \pm 6 \times 10^{-8}$	$159.8 \pm 9.3 \times 10^{-8}$
0.5	22.6 ± 1.1	14.4 ± 1.9
1.0	47.8 ± 2.4	567.4 ± 182
1.5	49.1 ± 5.5	679.1 ± 213
2.0	50.0 ± 6.9	796.6 ± 308
3.0	74.7 ± 16.5	2748.9 ± 1724

hydrogen bonded ensemble. From this observation, it can be inferred that there is a presence of a large scale structure in the Pd_8S-*co*-VPh/ LCPU blend, due to intra-species interactions within the VPh segments of the copolymer; an arrangement that is measurably disrupted by addition of the small amounts of LCPU, with a reduced Debye−Bueche correlation length of 22.5 nm. Further addition of LCPU to the blend results in an increase in the correlated size of the dynamic network, as well as zero scattering intensity $d\Sigma/d\Omega(0)$. One way to account for these increases is by allowing the LCPU molecules to integrate within the dynamic network. This possibility is supported by the fact that the carboxylic groups present on the LCPU molecules should readily form hydrogen bonds with the hydroxyl groups on the VPh segments.[17]

FTIR of Blends. To develop a quantitative interpretation of the nature of the hydrogen-bonding present within the LCPU−copolymer blends, Fourier transform infrared spectroscopy (FT-IR) was performed on the pure copolymer and its LCPU blends.[17,18,20] The FT-IR spectra of the Pd_8S-*co*-VPh/LCPU blends fail to show any perceptible carbonyl peaks due to the low concentration of LCPU in the blends. This is due to the very low concentrations of the LCPU, in addition to the fact that the measurement in the range of 1800 to 1650 cm^{-1} is obscured by low signal-to-noise ratio. Consequently, the analysis of the hydroxyl (−OH) stretching bands that occur between 3700 and 3100 cm^{-1} were completed.[53] These vibration bands are broad and suffer from overlap; therefore in order to analyze them, a Gaussian deconvolution curve fitting procedure was adopted. Accordingly, PeakFit application was used in the 3700 and 3000 cm^{-1} region of the spectra. In the curve fitting procedure, the principle of parsimony with regards to the number of peaks was employed. In other words, attempts were made to best fit the spectra, while allowing the minimum number of peaks.

The FT-IR spectra due to the pure copolymer and its blends are shown in Figure 10. The peak observed near 3010 cm^{-1} is due to aromatic C−H stretch bonds and is not relevant to our analysis. The remaining portion of the spectrum is deconvoluted. In the case of the neat copolymer, the spectrum is sufficiently deconvoluted with no more than two peaks. These peaks occur near 3552 and 3318 cm^{-1} (see Table 2). The first peak is due to −OH stretching from "free" hydroxyl groups. This peak retains the characteristic sharpness observed in "free" −OH stretch of phenols.[54] As the concentration of phenol groups in this experiment is considerably high, an additional peak due to the "associated" −OH stretch is observed. These vibrations occur due to −OH groups that are under the influence of hydrogen bonding among the vinylphenol segments.[53,55−57] The blends of LCPU and the Pd_8S-*co*-VPh copolymer register an additional peak in their FT-IR spectra that occurs in the region of 3452 cm^{-1}. This peak is due to the hydroxyl groups participating in inter-species hydrogen bonding with carbonyl groups of the LCPU.[53] This additional interaction appears at higher wavenumber than other −OH interactions, indicating that the inter-species hydrogen bonds are weaker than intra-species

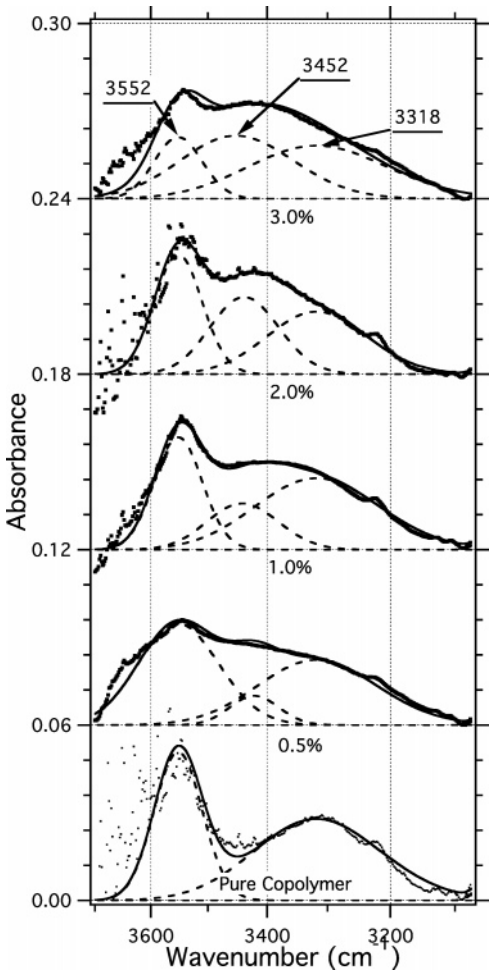

Figure 10. FT-IR absorbance spectra for Pd_8S-*co*-VPh copolymer and its blends containing 0.5−3% LCPU, together with Gauss deconvolution fit (—) and contributing peaks (- -), corresponding to "free" −OH group and inter-species hydrogen bond associated and intra-species hydrogen bond associated −OH groups, in order of decreasing wavenumbers.

Table 2. Curve-Fitting Results for FT-IR Spectra of Pd_8S-*co*-VPh/ LCPU Blends

LCPU content (wt %)	"free" −OH group		inter-species associated −OH groups		intra-species associated −OH groups	
	peak (cm^{-1})	area (cm^{-1})	peak (cm^{-1})	area (cm^{-1})	peak (cm^{-1})	area (cm^{-1})
0	3552	5.352		0	3318	7.193
0.5	3552	6.100	3433	1.034	3318	5.411
1.0	3552	4.020	3441	2.599	3318	5.927
2.0	3552	4.305	3483	3.860	3318	4.380
3.0	3552	2.219	3452	5.193	3318	5.132

hydrogen bonds.[57] Table 2 shows the peaks (and their area) due to "free" , "intra-species" , and "inter-species" −OH groups. The absolute values of these spectra are dependent on the path length; as a result the spectra were normalized, such that the total area under all the −OH stretch peaks is the same. (Note the concentration of −OH groups in the pure Pd_8S-*co*-VPh copolymer and all its blends is effectively the same; as the copolymer composition is kept the same and the LCPU content is very small.)

Table 3 shows the ratio of the area under each of these vibration bands to the cumulative area under all the −OH peaks. Although, this ratio cannot be taken directly as a quantitative measure of the concentrations of each type of −OH groups because the coefficient of absorption for different −OH stretches

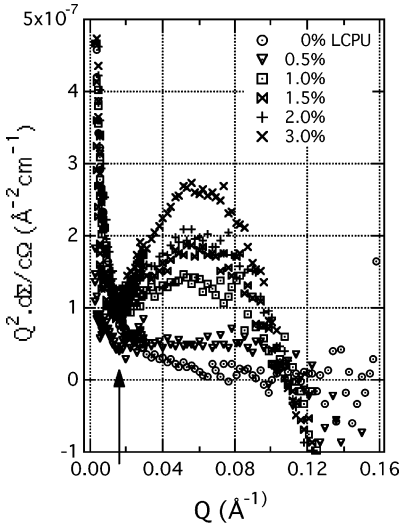

Figure 11. Kratky plot for neat Pd_8S-*co*-VPh copolymer and its blends containing 0.5 to 3% LCPU as a function of Q. SANS intensity for blends show excess scattering occurring at $Q > 0.016$ Å^{-1}, when compared with scattering from pure copolymer.

Table 3. Approximate Fractional Areas under Various −OH Peaks

	fractional area		
LCPU content (wt %)	"free" −OH group	inter-species associated −OH groups	intra-species associated −OH groups
0	0.427	0	0.573
0.5	0.487	0.0824	0.431
1.0	0.320	0.207	0.472
2.0	0.343	0.308	0.349
3.0	0.177	0.414	0.409

vary.[58] Nonetheless, only the ratio of the areas under the peaks is presented here and can be considered a qualitative estimate of ratios of the actual −OH concentrations. We can see from Table 3 that with the addition of the LCPU to the copolymer there is a progressive increase in the "inter-species" interaction, and an overall reduction of the "intra-species" interactions, occurring at the expense of "free" hydroxyl groups. Furthermore, it is clear that at the lowest LCPU dose, i.e., 0.5% LCPU content, the "free" hydroxyl group population increases, accompanied by a corresponding loss in "intra-species" interactions. This trend seems to reverse with increasing amounts of LCPU.

The IR thus indicates that in the 0.5% LCPU blend there is a disruption in the intra-species hydrogen bonding, which correlates well with the reduction in the scattering and the Debye−Bueche correlation length from 27.3 to 22.5 nm. Addition of more LCPU from 1 to 3 wt %, results in an increase in the Debye−Bueche correlation length from 47.8 to 74.7 nm, a 2−3-fold increase when compared to the correlation length in the neat copolymer. This observation is corroborated by an increase in the inter-species interaction, i.e., hydrogen bonding between VPh and LCPU molecules (Table 3); this serves as a confirmation of the integration of the LCPU molecules within the vinylphenol network. It should be noted that the FTIR measurements are made at room temperature, whereas the SANS measurements were made at 180 °C, and therefore, it is not possible to directly correlate the hydrogen bond distributions measured by FTIR with the scattering observations.

Mid-High *Q* SANS. To analyze the scattering data in the mid-high Q region, the data is plotted in the Kratky representation in Figure 11. Similar to Figure 4, the tail of the curve forms a plateau in the case of the scattering from neat polymer and shows a bell-shaped peak in the case of the scattering from the blends.

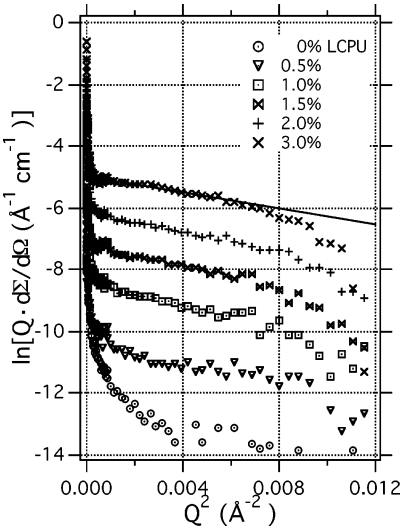

Figure 12. Logarithm of the first moment of SANS intensity for 0.5−3% LCPU−Pd_8S-*co*-VPh copolymer blends as a function of Q^2, to obtain the linear fit (—) to the Kratky−Porod wormlike chain model. The fit for only the 3% blend is shown. Data are offset for clarity. Data for the pure copolymer is also shown, which does not demonstrate linear behavior.

Table 4. Kratky−Porod Wormlike Chain Model Fitting Parameters

LCPU wt fraction (%)	$R_{g,x}$ (nm)	(M/L) (g/(mol nm))	L (nm)
0.5	1.95 ± 0.01	289 ± 18.4	114.1 ± 7.2
1.0	1.71 ± 0.007	325 ± 14.6	101.5 ± 4.6
1.5	1.67 ± 0.005	272 ± 8.7	121.5 ± 3.9
2.0	1.72 ± 0.003	233 ± 5.6	141.9 ± 3.4
3.0	1.69 ± 0.003	200 ± 4.0	164.9 ± 3.3

The broad peak observed in the Kratky plots due to the blends arises due to excess scattering from the LCPU molecules and displays KPWC behavior. Figure 12 shows the scattering data from the blends, plotted in Kratky−Porod representation $\{\ln[Q\mathrm{d}\Sigma(Q)/\mathrm{d}\Omega]$ vs $Q^2\}$. The linear nature of the scattering curve in the mid-high Q region (>0.016 Å^{-1}) provides further evidence of the presence of anisotropic structures in the blends. The linear fit provides a gradient that gives the cross-sectional radius of gyration of the rods $R_{g,x}$, which varies in its values from 1.95 to 1.67 nm (Table 4). The intercept provides the ratio M/L (the molecular weight per unit length along the anisotropic structure), which is a quantity that can be better interpreted in context to the molecular weight of the LCP molecules.

Utilizing the fact that the concentration of the LCP molecules, which are thought to be giving rise to the excess scattering in the mid-high Q region, is very small; a Zimm plot was prepared in order to determine the molecular weight of the LCP molecules.[59] The Zimm approximation appears as

$$\frac{1}{\frac{\mathrm{d}\Sigma}{\mathrm{d}\Omega}(Q)} = \frac{1}{k_1 cM}\left[1 + \frac{(QR_g)^2}{3}\right] + 2A_2k_2c \qquad (13)$$

where $k_1 = (\Delta\rho)^2/(N_A\delta^2)$, $k_2 = 1/k_1c$, A_2 the second virial coefficient, and $c = \delta\phi$, the concentration of the scattering molecules in the media. The Zimm plot is created by plotting $\{k_1c/[Q^2\mathrm{d}\Sigma(Q)/\mathrm{d}\Omega]\}$ vs $[c + \alpha Q^2]$, where α is an arbitrary scaling constant. The Zimm plot shows a family of parallel lines, extrapolation to $c = 0$ yields the R_g, and extrapolation to $Q = 0$ yields the A_2 and M.

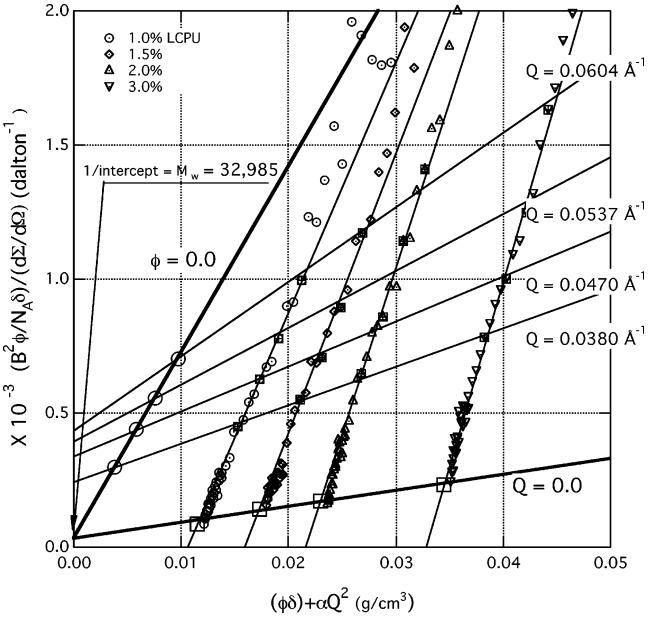

Figure 13. Zimm plot for LCPU/ Pd_8S-*co*-VPh blends containing 0.5−3% LCPU at 170 °C.

Although, the Zimm plot is customarily fitted to low Q region of the scattering curve; the low Q scattering (<0.016 Å^{-1}) in the case of Pd_8S-*co*-VPh and its blends is dominated by scattering arising from the hydrogen bonded VPh network. This portion of the scattering curve corresponds to the data to the left of the cusp in the Kratky plot, represented by the arrow in Figure 11. Data to the left of this arrow features a strong negative slope and represents the upturn in scattering. On the other hand, our interest is limited to the molecular information concerning individual anisotropic LCPU molecules, which is obtained from scattering data to the right of the arrow, which in the case of scattering from the blends manifests KPWC type behavior. As a result, for the purpose of the Zimm plot shown in Figure 13, scattering data only in the mid Q region ($0.016 < Q < 0.06$ Å^{-1}) is considered. Elsewhere, Zimm plots of cross-linked networks[52] and anisotropic polymers[60] show similar departure from the linear behavior in the low Q region.

The gradient of the line $c = 0$ yields R_g as 13.3 nm. The gradient of the line $Q = 0$ yields the $A_2 = 2.975 \times 10^{-3}$ mol cm^5/g^2. Intercepts of these two lines coincide within experimental error (32218^{-1} and 33789^{-1}) and their mean gives the molecular weight of 32985. The molecular weight of the LCPU measured by gel permeation chromatography GPC (using a polystyrene standard) was 31700.

The molecular weight of a repeat unit of the LCPU is 560. Assuming the entire repeat unit is stretched out end to end, the length of this repeat unit would be approximately 3.15 nm. A LCPU chain having molecular weight of 32985 would correspondingly extend over a length of approximately 185 nm. Also, the molecular weight per unit length of the repeat unit is 178 g mol^{-1} nm^{-1}, which is slightly smaller than the observed value of M/L provided by the KPWC model (200−325 g mol^{-1} nm^{-1}). If the anisotropic structures observed by SANS were composed of a single stretched out LCPU chain, the value of M/L should be in the vicinity of 178 g mol^{-1} nm^{-1}. The contrary observation suggests a bundling up of the rigid portions of the chain. This hypothesis is further supported by the observed thickness of the rods, which measured as the cross-sectional radius of gyration of the rods $R_{g,x}$ shows an average value of 1.6 nm, which is far larger than the radius of a single extended chain.

This structural information can be interpreted to provide insight into the conformation of the LCPU chain in the system. The structure of the LCPU molecules contains blocks of alkyl linkages [$-(CH_2)_6-$], which link up the rigid portions of the LCPU molecules (see Figure 1). These flexible spacer blocks are themselves connected to the rigid mesogens by ether linkages. As a result, the flexible alkyl spacers provide a degree of flexibility within the LCPU chain, which may allow the chain to take conformations that stagger its mesogens along the length of the anisotropic bundles, by exhibiting some long-range orientational order, and hence the anisotropy is observed. This chain structure will result in effectively shortening the LCPU repeat unit and increasing M/L when compared to a fully extended LCPU chain; consequently, the length of such a chain is shorter than the contour length that it would occupy if it were fully distended from end to end. If we assume that a given anisotropic structure contains repeat units from a single chain, the product of the molecular weight obtained from the Zimm plot and the M/L provided by the KPWC model results in the contour length of a LCPU chain L (right most column in Table 4), which represents the length of all anisotropic units along the chain put along a straight line.

In the case of dilute LCPU blends, where the probability of overlap between the LCPU is low, it is reasonable to assume that each anisotropic scattering unit is made up of only one chain. Therefore, for low LCPU content blends, increasing concentration of the LCPU, the $R_{g,x}$and the M/L decreases. Thus, it appears that increasing the LCPU concentration makes the anisotropic structures become thinner and leaner. This effectively results in increasing the contour length of the chain, but does not necessarily affect the length of any given anisotropic bundle. This can be understood as the result of the interference between different LCPU molecules, which causes the rods to orient under influence of each other and thereby producing structures with larger anisotropic sections.

The M/L observed in the blends containing 5 and 20% LCPU (436 and 572 g mol^{-1} nm^{-1} respectively) are significantly greater than those observed at lower concentrations increases. In fact, this value is greater than the $M/L = 178$ g mol^{-1} nm^{-1} of a single fully extended LCPU repeat unit. This leads to the inference that at higher LCPU loading, multiple LCPU molecules aggregate together forming anisotropic structures that are heavier than rigid rods formed of individual molecules observed in blends having lower LCPU concentrations. It should be noted that for these blend compositions the single chain assumption made earlier is no longer valid, and for such aggregates it is not possible to define a contour length.

Conclusions

Our ability to prepare miscible blends of liquid crystalline polymers (LCP) and flexible polymer, has presented us with an opportunity to investigate the conformation of the LCP molecule in an amorphous coiled polymeric matrix, in which it is uniformly dispersed. The high upturn in the small-angle neutron scattering at low Q indicates the presence of a dynamic network in the Pd_8S-*co*-VPh copolymer. The low Q scattering as well as FT-IR studies show clear evidence of hydrogen-bonding interactions between LCPU and the copolymer. The addition of LCPU to the PS-*co*-VPh succeeds in breaking down the network while simultaneously interacting with the network, forming new large-scale structures. The LCP molecules within the blend assume anisotropic conformations as indicated by successful fit to the Kratky−Porod wormlike chain model. The LCPU chains are composed of anisotropic bundles, with its rigid

mesogens staggered within their length, resulting in wormlike structures that are shorter and thicker than a fully extended LCPU chain.

Acknowledgment. The authors gratefully acknowledge The University of Tennessee Neutron Science Scholar Program and the National Science Foundation, Division of Materials Research, for financial support (DMR-024124), which funded this research. We thank the National Center for Neutron Research of the National Institute of Standard and Technology and the Institute of Solid State Research (IFF) of Forschungszentrum at Jülich, Germany, for beam time on the SANS instruments. We also thank D. Schwahn and H. Endo for their critical discussions and valuable technical assistance.

References and Notes

(1) Chandrasekhar, S. *Liquid Crystals*, 2nd ed.; Cambridge University Press: New York, 1992.
(2) Aceimo, D.; La Mantia, F. P. *Processing and Properties of Liquid Crystalline Polymers and LCP Based Blends*; ChemTec Publishing: Toronto, Canada, 1993.
(3) Wissbrun, K. F. *Br. Polym. J.* **1980**, *12*, 163−169. Wissbrun, K. F. *J. Rheol. (N.Y.)* **1981**, *25*, 619−662. Wissbrun, K. F.; Griffin, A. C. *J. Polym. Sci., Polym. Phys. Ed.* **1982**, *20*, 1835−1845.
(4) Cogswell, F. N. *Br. Polym. J.* **1980**, *12*, 170.
(5) Prasadarao, M.; Pearce, E. M.; Han, C. D. *J. Appl. Polym. Sci.* **1982**, *27*, 1343−1354.
(6) *Liquid Crystalline Polymers*; The Committee on Liquid Crystalline Polymers, National Materials Advisory Board, Commission on Engineering and Technical Systems, National Research Council: Washington, DC, 1990.
(7) Doane, J. W.; Golemme, A.; West, J. L.; Whitehead Jr., J. B.; Wu, B. G. *Mol. Cryst. Liq. Cryst.* **1988**, *165*, 511−532.
(8) Kaneko, E. *Liquid Crystal TV Displays: Principles and Applications of Liquid Crystal Displays*; Reidel: Boston, MA, 1987.
(9) Miyamoto, A.; Kikuchi, H.; Morimura, Y.; Kajiyama, T. *New Polym. Mater.* **1990**, *2*, 27−40. Miyamoto, A.; Kikuchi, H.; Kobayashi, S.; Morimura, Y.; Kajiyama, T. *Macromolecules* **1991**, *24*, 3915−3920.
(10) Shen, C.; Kyu. T. *J. Chem. Phys.* **1995**, *102*, 556−562.
(11) Hwang, W.-F.; Wiff, D. R.; Verschoore, C.; Price, G.; Helminiak, T. E..; Adams, W. W. *Polym. Eng.* Sci. **1983**, *23*, 784−788.
(12) Hwang, W.-F.; Wiff, D. R.; Benner, C. L.; Helminiak, T. E. *J. Macromol. Sci. (Phys.)* **1983**, *B22*, 231−257.
(13) Hwang, W.-F.; Wiff, D. R.; Verschoore, C. *Polym. Eng. Sci.* **1983**, *23*, 789−791.
(14) Pawlikowski, G. T.; Dutta, D.; Weiss, R. A. *Annu. Rev. Mater. Sci.* **1991**, *21*, 159−184.
(15) Isayev, A. I. In *Liquid Crystalline Polymer Systems: Technological Advances*; Isayev, A. I.; Kyu, T.; Cheng, S. Z. D.; Eds.; American Chemical Society: Washington, DC, 1996.
(16) Schartel, B.; Wendorff, J. H. *Polym. Eng. Sci.* **1999**, *29*, 128−151.
(17) Viswanathan, S.; Dadmun, M. D. *Macromol. Rapid Commun.* **2001**, *22*, 779−782.
(18) Viswanathan, S.; Dadmun, M. D. *Macromolecules* **2002**, *35*, 5049−5060.
(19) Radmard, B.; Dadmun, M. D. *Polymer* **2001**, *42*, 1591−1600.
(20) Viswanathan, S.; Dadmun, M. D. *Macromolecules* **2003**, *36*, 3196−3205.
(21) Gardlund, Z. G. *Polymer* **1993**, *34*, 1850−1857.
(22) Sato, A.; Kato, T.; Uryu T *J. Polym. Sci., Part A: Polym. Chem.* **1996**, *34*, 503−505.
(23) Khatri, C. A.; Vaidya, M. M.; Levon, K.; Jha, S. K.; Green, M. M. *Macromolecules* **1995**, *28*, 4719−4728.
(24) Painter, P. C.; Tang, W. L.; Graf, J. F.; Thomson, B.; Coleman, M. M. *Macromolecules* **1991**, *24*, 3929−3936.
(25) Weiss, R. A.; Ghebremeskel, Y.; Charbonneau, L. *Polymer* **2000**, *41*, 3471−3477.
(26) Tsou, L.; Sauer, J. A.; Hara, M. *Polymer* **2000**, *41*, 8103−8111.
(27) Parker, G.; Hara, M. *Polymer* **1997**, *38*, 2701−2709.
(28) Tsou, L.; Sauer, J. A.; Hara, M. *J. Polym. Sci., Part B: Polym. Phys.* **2000**, *38*, 1369−1377; **2000**, *38*, 1377−1385.
(29) Weiss, R. A.; Shao, L.; Lundberg, R. D. *Macromolecules* **1992**, *25*, 6370−6372.
(30) Flory, P. J. *Proc. R. Soc. London* **1956**, *A234*, 60−73.
(31) Flory, P. J. *Macromolecules* **1978**, *11*, 1138−1141.
(32) Tang, W. L.; Coleman, M. M.; Painter, P. C. *Macromol. Symp.* **1994**, *84*, 315−324.
(33) Higgins, J. S.; Benoit, H. C. *Polymers and Neutron Scattering*; Clarendon Press: Oxford, U.K., 1994.
(34) Gilra, N.; Cohen, C.; Briber, R. M.; Bauer, B. J.; Hedden, R. C.; Panagiotopoulos, A. Z. *Macromolecules* **2001**, *34*, 7773−7782.
(35) Brûlet, A.; Fourmaux-Demange, V.; Cotton, J. P. *Macromolecules* **2001**, *34*, 3077−3080.
(36) Noirez, L.; Ungerank, M.; Stelzer, F. *Macromolecules* **2001**, *34*, 7885−7893.
(37) Hardouin, F.; Sigaud, G.; Achard, M. F.; Brulet, A.; Cotton, J. P.; Yoon, D. Y.; Percec, V.; Kawasumi, M. *Macromolecules* **1995**, *28*, 5427−5433.
(38) Cotton, J. P.; Hardouin, F. *Prog. Polym. Sci.* **1997**, *22*, 795−828.
(39) Arrighi, V.; Higgins, J. S.; Weiss, R. A.; Cimecioglu, A. L. *Macromolecules* **1992**, *25*, 5297−5305.
(40) Debye, P.; Bueche, A. M. *J. Appl. Phys.* **1949**, *20*, 518−525.
(41) Benoit, H.; Joanny, J. F.; Hadziioannou, G.; Hammouda, B. *Macromolecules* **1993**, *26*, 5790−5795.
(42) Kratky, O.; Porod, G. *Recl. Trav. Chim. Pays-Bas* **1949**, *68*, 1106−1122.
(43) Stenhouse, P. J.; Valles, E. M.; Kantor, S. W.; MacKnight, W. J. *Macromolecules* **1989**, *22*, 1467−1473.
(44) Percec, V.; Kim, H.-J.; Barboiu, B. *Macromolecules* **1997**, *30*, 6702−6705.
(45) Eastwood, E. A.; Dadmun, M. D. *Macromolecules* **2001**, *34*, 740−747.
(46) Russell, T. P.; Ito, H.; Wignall, G. D. *Macromolecules* **1988**, *21*, 1703−1709.
(47) Marr, D. W. M. *Macromolecules* **1995**, *28*, 8470−8476.
(48) Debye, P. *J. Phys. Colloid Chem.* **1947**, *51*, 18−32.
(49) Coleman, M. M.; Graf, J. F.; Painter, P. C. *Specific Interactions and the Miscibility of Polymer Blends*; Technomic: Lancaster, PA, 1991; pp 191−194, 283−385.
(50) Fazel, N.; Brulet, A.; Guenet, J.-M. *Macromolecules* **1994**, *27*, 3836−3842.
(51) Saiani, A.; Guenet, J.-M. *Macromolecules* **1997**, *30*, 966−972.
(52) Pyckhout-Hintzen, W.; Springer, T.; Forster, F.; Gronski, W.; Frischkorn, C. *Macromolecules* **1991**, *24*, 1269−1274.
(53) Li, D.; Brisson, J. *Polymer* **1998**, *39*, 793−800.
(54) Silverstein, R. M.; Webster, F. X. *Spectroscopic Identification of Organic Compounds*, 6th ed.; John Wiley and Sons Inc.: New York, 1998; p 87−90.
(55) Moskala, E. J.; Varnell, D. F.; Coleman, M. M. *Polymer* **1985**, *26*, 228−234.
(56) Kuo, S. W.; Huang, C. F.; Chang, F. C. *J. Polym. Sci.: Polym. Phys. B* **2001**, *39*, 1348−1359.
(57) He, Y.; Li, J.; Uyama, H.; Kobayashi, S.; Inoue, Y. *J. Polym. Sci.: Polym. Phys. B* **2003**, *39*, 2898−2905.
(58) Coleman, M. M.; Lee, K. H.; Skrovanek, D. J.; Painter, P. C. *Macromolecules* **1986**, *19*, 2149−2157.
(59) Kirste, R. G.; Kruse, W. A.; Ibel, K. *Polymer* **1975**, *16*, 120−124.
(60) MacDonald, W. A.; McLenaghan, A. D. W.; Richards, R. W. *Macromolecules* **1992**, *25*, 826−831.

MA0610360